

Computational impact responses of reinforced concrete slabs

S.N. Mokhatar¹, R. Abdullah² and A.B.H. Kueh^{*3}

¹*Department of Civil Engineering, Faculty of Civil and Environmental Engineering, Universiti Tun Hussein Onn Malaysia, 86400 Parit Raja, Johor, Malaysia*

²*Department of Structure and Materials, Faculty of Civil Engineering, Universiti Teknologi Malaysia, 81310 Skudai, Johor, Malaysia*

³*Construction Research Centre, Universiti Teknologi Malaysia, 81310 Skudai, Johor, Malaysia*

(Received February 17, 2012, Revised October 18, 2012, Accepted October 27, 2012)

Abstract. The responses of reinforced concrete slabs subject to an impact loading near the ultimate load range are explored. The analysis is carried out on a simply supported rectangular reinforced concrete slab using a nonlinear explicit dynamic procedure and considering three material models: Drucker-Prager, modified Drucker-Prager, and concrete damaged plasticity, available in the commercial finite element software, ABAQUS/Explicit. For comparison purposes, the impact force-time response, steel reinforcement failure, and concrete perforation pattern are verified against the existing experimental results. Also, the effectiveness of mesh density and damage wave propagation are studied independently. It is shown that the presently adopted finite element procedure is able to simulate and predict fairly accurate the behavior of reinforced concrete slab under impact load. More detailed investigations are however demanded for the justification of effects coming from an imperfect projectile orientation as well as the load and structural surface conditions, including the impulsive contacted state, which are inevitable in an actual impact environment.

Keywords: impact load analysis; reinforced concrete slab; finite element; explicit dynamics analysis; perforation

1. Introduction

Structural response and resistance of reinforced concrete structures under the influence of a harsh dynamic environment, especially the impact load, are gaining research attention in recent years due to their paramount importance. Examples of events in the presence of such loading are vehicle crashes onto the bridge parapet wall, ice and ship collisions with the marine and offshore structures as well as shock and blasting impacts on structures in close proximity, just to name a few. These loadings can be considerably severe since impact loads, which naturally occur in a split of second, exert damaging magnitude many times that of their static equivalence of the same mass.

*Corresponding author, Ph.D., E-mail: kbhahmad@utm.my

To date, experiment is possibly the best method for studying the response of a structure under impact loading. However, experiment alone is not sufficient for the entirety of investigation due to difficulties in measuring the responses of structures at a very short period of time, particularly near the ultimate load range. Also, experimental studies can be costly and extensively laborious if many parameters are to be explored. Due to these factors, computer simulation is needed as a cheaper alternative for assessing the response of structures under impact loading. In the past, efforts for assessing and predicting the behavior of concrete structures subjected to impact loads were hampered by the lack of adequate analytical procedure, unavailability of good computer software, and slow computing capability.

The advancement of computational capability in exponential manner has led the numerical modeling to rapidly become indispensable and taken complementary and essential roles in the exploration of the mechanical response of large structures, which can at times be costly and tedious when examined via the experimental approach. For convenience and cost effectiveness, numerical models, such as the finite element (FE), have been made available and broadly used in the investigation of reinforced concrete (RC) slabs under the influence of impact load. Amongst the earliest works concerning the modeling of RC slabs was carried out by Jofriet and McNeice (1971). They considered the slab as an elastic material, in which the bilinear moment-curvature relation is obtained from the effective second moment of area of a cracked slab section, which includes also the tension stiffening behavior. A progressive crack through the thickness was modeled by Hand *et al.* (1973) using the finite element method through the discretization of slab in a layered manner. Similar approach can be tracked in Scanlon and Murray (1974) in which additional effects of the shrinkage and creep in slabs were considered, assuming that only an orthogonal crack trajectory is permitted. The elasto-plastic material expressions for concrete and reinforcement were considered by Lin and Scordelis (1975), utilizing a layered shell element that incorporates the axial and flexural coupling effects and the tension stiffening of concrete between cracks. In modeling the interaction of reinforced concrete, there exist three primarily adopted descriptions in literatures: smeared, embedded, and discrete models. The most extensively applied being that of smeared type, attributable to its simplicity and less detailed nature. It was originally proposed by Rashid (1968) in the research of prestressed concrete reactor structures. The smeared method approximates the reinforcement mesh by modeling it as a composite layer in the concrete using the lumped properties. The representation, although general, has found warm acceptance and consequently a great amount of effort being devoted in the improvement and revision of its functionality (Abbas *et al.* 2004, Gilbert and Warner 1978, Lin and Scordelis 1975). The embedded model was introduced by Phillips and Zienkiewicz (1976), treating the reinforcing bar as an axial member implanted in a 2D isoparametric element that is used to model the concrete. The formulation has since been rigorously upgraded to exhibit the bond-slip capability (Balakrishnan and Murray 1986), allowing for curved steel bars insertion (Elwi and Hruday 1989), and several modifications in regard to the positioning of reinforcements with respect to the natural axis of concrete element to reduce input requirement (Zienkiewicz *et al.* 1972). An interaction between different shear link, steel bar, and concrete has been established using the embedded model in the study of RC slab response due to impact loads (Tahmasebinia 2008). To model detailed localized effects, the discrete formulation is more appropriate (Rousseau *et al.* 2009; Sawamoto *et al.* 1998, Shiu *et al.* 2009). This approach models the reinforcement discretely as truss or beam elements attached to the concrete at a set of common nodes. An expensive computational cost may be imposed owing to a massive concrete mesh refinement to accommodate the rearrangement of steel bars and cracks. Due to the computational cost, most of

these studies have regarded only two-dimensional model. For thorough discussion on the issues of three-dimensional modeling of reinforced concrete structures using the finite element approach, the work by Gomes and Awruch (2001) can be referred. Furthermore, a review of major analytical and experimental works on the impact loading on plates and shells by projectiles can be found in Corbett *et al.* (1996). A variant of explorations of the impact load effects on concrete slabs in terms of the short fibrous type reinforcement were presented in Ong *et al.* (1999) and Naaman and Gopalaratnam (1983). In much the same vein, a great amount of attention has been pointed to the simulation of high velocity impact on RC slabs that considers also the perforation of the impacted medium. Agardh and Laine (1999) simulated, with the material data input from relevant experimental works obtained from literature, the high velocity fragment perforation of RC slabs in a 3D environment using the commercial FE package LS-DYNA that incorporates the material model with an erosion feature. A 2D equivalent inclusion plane strain FE model was used by Teng *et al.* (2004) to investigate the penetration depth and residual velocity of projectile when it is impacted on RC targets. Associated equivalent material moduli were obtained using the Mori–Tanaka’s average strain theory and the equivalent stiffness matrix of homogenized concrete-steel material for finite element analyses. Via similar modeling approach, Teng *et al.* (2005) examined the penetration resistance of RC containment structures where a phase diagram for design purpose was produced from the modeled outputs to describe the correlation of the projectile striking angle and target thickness. In regard to the impact resistance, Chen *et al.* (2008) in a separate study found that the reinforcement ratio of concrete and tensile strength of reinforcement are the primary factors affecting the perforation process. For the determination of the origin of explosion and mass of explosive used, a concrete pavement slab under the blast loads was studied by Luccioni and Luege (2006) through a variation in the amount of explosive used and its elevation from the ground. By the FE simulation and employing the Johnson–Holmquist concrete material constitutive law, Tai and Tang (2006) and Islam *et al.* (2011) examined the reinforced concrete structural dynamic response and failure behavior when subjected to different velocities of projectile impact. They observed that the reinforced concrete failure and deceleration of projectile depend very much on the impact velocity. The effects of the types of slab reinforcement and applied impact loads on the dynamic response of reinforced concrete slabs were explored by Zineddin and Krauthammer (2007) in the experimental environment. The steel reinforcement amount and quality as well as the impact load height were reported to have an effect on the failure mode of slabs. It is essential to note that the aforementioned reviewed works studied the structural responses of RC slabs under the influence of impact load using mainly two-dimensional models. This is chiefly due to the modeling complexity and high computation time consumption of the three-dimensional solid model especially in the study of problems of dynamic nature. Nevertheless, a contribution has been made in the study of three-dimensional nonlinear finite element analysis of reinforced concrete targets under impact loading conducted by Abbas *et al.* (2004), in which the reinforced concrete was modeled with the strain rate sensitive elastoviscoplastic two surface model. With regard to solid element models, an improved accuracy and simulation set-up can be achieved with a better modeling judgment. It is essential to state here that to achieve a numerical work that is compatible with observation and since the effort on 3D simulation is scant in publication, there exists urging need to address the 3D deformation pattern of impacted medium in order to have an unrestricted comprehension of structural response that is inhibited by previous modeling approach, focusing on behavior on only single plane.

In the present study, the responses of simply supported rectangular reinforced concrete slabs subjected to an impact loading near the ultimate load range are numerically analyzed. The analysis

is performed using the commercial finite element software package ABAQUS/Explicit (ABAQUS, 2007), in which a nonlinear explicit dynamic procedure is employed.

2. Structural description

For convenience, we numerically explore in the current study the impact tests carried out at the Heriot-Watt University in Edinburgh by Sangi and May (2009) and Chen and May (2009) concerning the high mass – low velocity impact behavior of reinforced concrete slab. The details of the tests are therefore given herein. The tests were carried out on several slab specimens under drop-weight loads. The slabs were square and supported with steel frames at all sides. The slabs' size was 760 mm by 760 mm in terms of their surface area and 76 mm in depth whereas the effective concrete region was 725 mm by 725 mm by 76 mm. The top and bottom reinforcements of slab comprised meshes of 6 mm diameter high yield steel bars spaced at 60 mm intervals. The concrete cover between the main reinforcement bars and the top and bottom edges of the slab was given as 12 mm. For impact loading, a flat nose cylindrical projectile of circular cross-section with a diameter of 100 mm and a weight of 98 kg was used.

3. Computational modeling

We have previously mentioned, in the literature review, that the reinforced concrete structures can be modeled using the smeared, embedded, and discrete approaches. In the current work, we shall be interested in the embedded modeling technique. We shall also submit the simulation of reinforced concrete using three dimensional solid finite elements since a full spatial structural response is of primary concern. Detailed modeling treatments of the RC slab in the presence of impact load are provided in the followings.

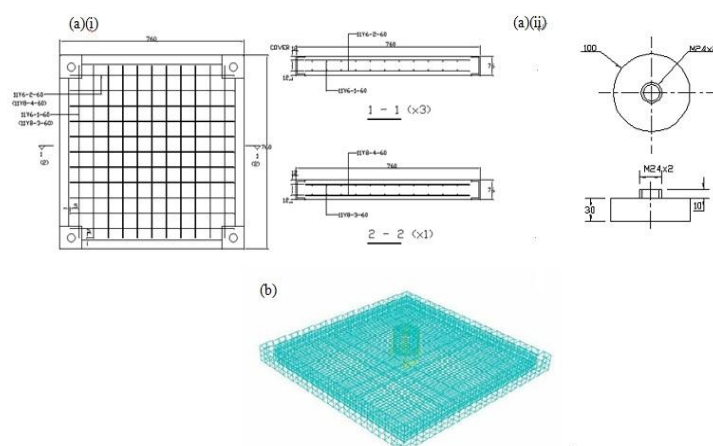


Fig. 1 (a) Plane and side schematics of experimental specimens (Sangi and May 2009, Chen and May 2009), (i) reinforced concrete (RC) slab and (ii) drop weight (b) corresponding rendered (wireframe) model used in the current simulation

3.1 Element definition

The experimental specimen (Sangi and May 2009, Chen and May 2009) and the rendered view of model used in the current study are illustrated in Fig. 1. To model the RC slab and steel bars details, the choices of elemental discretization are presented as follows. Firstly, the eight-node linear brick continuum elements with a reduced integration scheme (C3D8R) are created for the slab adopting three different material descriptions: Drucker-Prager (DP), modified Drucker-Prager (MDP) and concrete damaged plasticity (CDP). Secondly, the steel reinforcements are modeled with two-node space beam elements (B31), end nodes of which are connected to the nodes of adjacent solid elements using the embedded approach. In addition, 6 mm diameter is prescribed for both the top and bottom reinforcements. There are in total 5280 beam elements and 5082 nodes for the reinforcements. To model the steel supports surrounding the perimeter of RC slab, the discrete rigid element is used. Finally, the steel projectile that is used to prescribe the impact load is meshed with the continuum solid elements (C3D8R), which are by symmetry revolved 360° to produce the cylindrical shape. A total 413 solid elements and 576 nodes are employed for the projectile. Note that the behavior of projectile is mesh-independent since a rigid assumption is made and its deformation is not under consideration in this paper. In addition, the hourglass control and mesh distortion control techniques are used in the simulation.

3.2 Interaction

It is essential to note that individually modeled elements should be connected to each other in terms of appropriately defined interaction after the assembly of structural and non-structural elements. The contact type *TIE is utilized to model the interactions between un-deformable discrete rigid elements (steel support at all sides) and solid elements (concrete slab). It offers an equalization of the global displacements and rotations as well as all other active degrees of freedom at two connecting nodes, which is a reasonable description for the currently considered problem since it avoids the shear interaction between two elements. In this investigation, the embedded technique is used to constraint the beam elements (steel reinforcements) located within the solid element (concrete slab) in order to create a proper bonding action. Note that the constrained nodes need not necessarily be at the same location, hence, the embedded definition. The embedded technique ensures that the translational degrees of freedom of the embedded nodes, i.e., the nodes of rebar are constrained to the interpolated values of the corresponding degrees of freedom of the solid element. The surface-to-surface contact with an explicit scheme is defined for the interaction between the impact load and concrete slab. Furthermore, the kinematic contact method prescribed by the mechanical constraint formulation is utilized in defining the contact behavior during impact. A friction coefficient of 0.2 is used for all contact surfaces.

3.3 Material models

3.3.1 Strain rate decomposition

In the current model, the linear strain rate decomposition is employed such that a superposition of the elastic and time independent plastic strain rates is possible for the prescription of the total strain rate. For convenience, we assume the vanishing of time dependent creep strain rate from our model description.

3.3.2 Elastic and plastic behaviors

We consider in our model independently described elastic and plastic behaviors for the concrete and steel bars. Linear elastic properties have been adopted for the elastic behavior of both materials which are respectively summarized in Table 1. The plastic hardening parameters are presented in a tabulated form for the steel reinforcement in Table A1 in Appendix. In terms of the plastic behaviors, the frictional material like currently considered concrete is commonly expressed using the Drucker-Prager plasticity model (DP). For this material expression, *DRUCKER PRAGER is utilized in this study. We will also investigate in addition the use of brittle-cracking material or concrete damaged plasticity (CDP) for the slab. Furthermore, a modified version of the Drucker-Prager plasticity model (MDP) introduced by DiMaggio and Sandler (1971) that includes a cap to express a nonlinear relation between the hydrostatic stress and volumetric strain is employed. The chief intention here is to evaluate the impact force history produced by each material model when compared upon that obtained from the experimental study, the best of which is later further investigated in the failure modeling of slab. Thus, it is also useful for convenience of the mathematical modeling and comprehensive understanding to present all corresponding material expressions so that the function of the given material parameters listed hereafter can be well appreciated and correlated to their fundamental descriptions. The yield surface of DP conveniently takes the form of three stress invariants: the equivalent pressure stress, the Mises equivalent stress, and the third deviatoric stress invariant respectively given as

$$p = -\frac{1}{3} \text{trace}(\sigma), \quad q = \sqrt{\frac{3}{2} (\mathbf{s} : \mathbf{s})}, \quad \text{and} \quad r = \left(\frac{9}{2} \mathbf{s} \cdot \mathbf{s} : \mathbf{s} \right)^{\frac{1}{3}} \quad (1)$$

Here, σ are the stress components and S are the deviatoric stresses

$$S = \sigma + pI \quad (2)$$

The yield criterion for DP is customarily represented as

$$F = t - p \tan \beta - d = 0 \quad (3)$$

where β and d are the angle of friction of the material and its cohesion, respectively. t , the deviatoric stress measure, can be obtained as

$$t = \frac{q}{2} \left[1 + \frac{1}{K} \right] - \left(1 - \frac{1}{K} \right) \left(\frac{r}{q} \right)^3 \quad (4)$$

where K is the material parameter that shapes the yield surface in the deviatoric plane. It is important to state that for convexity of the yield surface, $0.778 \leq K \leq 1.0$.

To describe the yield surface of MDP, *CAP PLASTICITY, couples with the Drucker-Prager material model as well as the transition region in between, of ABAQUS/Explicit have been employed. The resulting yield surface comprises three major parts: shear, transition, and cap surfaces. The shear failure surface resumes the same form as given in Eq. (4). The transitional yield surface which links the shear failure surface to that of the cap is defined by

$$F_t = \sqrt{[p - p_a]^2 + \left[t - \left(1 - \frac{a}{\cos \beta} \right) (d + p_a \tan \beta) \right]^2} - a(d + p_a \tan \beta) = 0 \quad (5)$$

Table 1 Concrete and reinforcement elastic material properties

Concrete					
Young's modulus, E_c	Poisson's ratio, ν_c	Density, ρ_c	Fracture energy, G_c	Compression strength, f_{cu}	Tensile strength, f_{ct}
[N/m ²]		[kg/m ³]	[N/m]	[N/mm ²]	[N/mm ²]
3.00E+10	0.2	2400	100	53	2.1
Reinforcement					
Young's modulus, E_s	Poisson's ratio, ν_s	Density, ρ_s	Yield stress, f_y	Ultimate stress, f_u	
[N/m ²]		[kg/m ³]	[N/m ²]	[N/m ²]	
2.1E+11	0.29	7800	5.60E+08	6.30E+08	

α ensures a smooth transition between the shear and cap surfaces. p_a is an evolution parameter that represents the volumetric plastic strain driven hardening/softening. It can be expressed as

$$p_a = \frac{p_b - R_d}{(1 + R \tan \beta)} \quad (6)$$

R is the material eccentricity parameter that shapes the cap yield surface. $p_b(\varepsilon_{|0}^{\text{in}} + \varepsilon^{\text{pl}})$ is the hydrostatic compression yield stress. $\varepsilon_{|0}^{\text{in}}$ and ε^{pl} are the volumetric initial inelastic and plastic strains. The cap yield surface takes the following form

$$F_c = \sqrt{[p - p_a]^2 + \left[\frac{Rt}{1 + \alpha - \alpha / \cos \beta} \right]^2} - R(d + p_a \tan \beta) = 0 \quad (7)$$

The cap yield surface, which includes the dependence on the third stress invariant in the deviatoric plane, has an elliptical shape with a constant eccentricity in the p - t plane. The surface hardens or softens in accordance with the volumetric inelastic strain. Note that the volumetric plastic compaction and dilation cause hardening and softening, respectively.

For CDP model, relationships analogous to Eqs. (1)-(2) are used. The variables are differing however in that the effective descriptions are adopted here. In ABAQUS, *CONCRETE DAMAGED PLASTICITY has been employed for this material model. The yield relation to note is that considers distinctive tensile and compressive strengths expressed below as

$$F = \frac{1}{1 - \alpha} \left(\bar{q} - 3a\bar{p} + \beta(\bar{\varepsilon}^{\text{pl}})(\hat{\sigma}_{\text{max}}) - \gamma(-\hat{\sigma}_{\text{max}}) \right) - \bar{\sigma}_c(\bar{\varepsilon}^{\text{pl}}) = 0 \quad (8)$$

where

$$a = \frac{\left(\frac{\sigma_{b0}}{\sigma_{c0}} \right) - 1}{2 \left(\frac{\sigma_{b0}}{\sigma_{c0}} \right) - 1}; \quad 0 \leq \alpha \leq 0.5, \quad \beta = \frac{\bar{\sigma}_c(\bar{\varepsilon}_c^{\text{pl}})}{\bar{\sigma}_t(\bar{\varepsilon}_t^{\text{pl}})} (1 - \alpha) - (1 + \alpha), \quad \text{and} \quad \gamma = \frac{3(1 - K_c)}{2K_c - 1} \quad (9)$$

Now, $\hat{\sigma}_{\max}$ is the maximum principal effective stress, σ_{b0}/σ_{c0} is the ratio of initial equibiaxial compressive yield stress to that of initial uniaxial, and K_c is the ratio of the second stress invariant on the tensile meridian to that on the compressive meridian. σ_t and σ_c are respectively the effective tensile and compressive cohesion stresses.

It is well established in the theory of plasticity that the plastic flow rule is the relation that defines the change in plastic strains. Here, the flow potential for DP is defined by

$$G = t - p \tan \psi \quad (10)$$

where ψ is the dilation angle measured in the p - q plane. We adopt here for MDP the plastic flow that takes the yield surface as the potential function in the deviatoric plane (associated). This is similarly defined for the cap region in the meridional plane whereas a non-associated relation is used in those of shear and transition regions in the meridional plane. The cap region of the flow potential surface in the meridional plane takes the form

$$G_c = \sqrt{[p - p_\alpha]^2 + \left[\frac{Rt}{1 + \alpha - \alpha / \cos \beta} \right]^2} \quad (11)$$

The shear region can be described by the following

$$G_s = \sqrt{[(p_\alpha - p) \tan \beta]^2 + \left[\frac{t}{1 + \alpha - \alpha / \cos \beta} \right]^2} \quad (12)$$

Table 2 Material properties for yield surface definition

Drucker-Prager model parameters					
Angle of friction, β		Flow stress ratio, K		Dilation angle, ψ	
30°		1		20°	
Modified Drucker-Prager model parameters					
Material cohesion, d [N/m ²]	Material angle of friction, β	Cap eccentricity parameter, R	Initial cap yield surface position	Flow stress ratio, K	Strain rate
4705672	51°	0.65	0.0011	1	1.5
Concrete damaged plasticity model parameters					
Dilation angle	Eccentricity, ε	σ_{b0}/σ_{c0}	K_c	Viscosity parameter, μ	
38°	1	1.12	1	0.666	

Table 3 Number of elements and nodes for each case of slab meshes

Mesh type	Number of solid elements	Number of nodes	Through thickness solid elements number
Mesh I	100	242	1
Mesh II	11520	14406	5
Mesh III	41472	47961	8

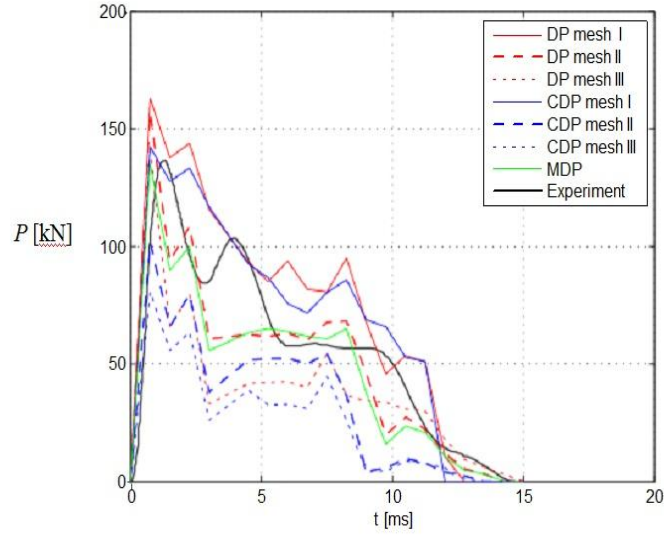


Fig. 2 Impact force-time relations for models and experiment

For CDP model, the plastic flow rule definition is that of non-associative type and the potential function used can be stated as

$$G = \sqrt{(\varepsilon \sigma_{t0} \tan \psi)^2 + \bar{q}^2} - \bar{p} \tan \psi \quad (13)$$

σ_{t0} is the uniaxial tensile stress at failure obtained from the tensile behaviors and ε is the eccentricity that characterizes the asymptote approaching rate of flow potential function. To circumvent severe convergence issue typically found in the material with softening nature, viscoplastic regularization of the constitutive equations utilizing a viscosity parameter, μ , is exercised to ensure a positive consistency of the tangent stiffness of the softening and stiffness degraded material for adequately small time increments (ABAQUS 2007).

For the prescriptions of parameters for the aforementioned yield surfaces, the input data that conform to the works presented in Tahmasebinia (2008), Sangi and May (2009) and Chen and May (2009) are listed in Table 2. These variables have been defined and expressed in Eqs. (1-2). Note that $K = 1$ since ABAQUS/Explicit allows only such flow stress ratio (ABAQUS 2007). Also, the DP yield surface customarily gives greater shear strength under a large compressive confining (hydrostatic) pressure such that there is no limitation in the compression region. Since the prediction of the behavior of cementitious materials like concrete depends very much on their compressive conditions, a high dependency on the confining pressure without the volumetric control influences their real behavior under a high impact load environment. To reduce the shear estimation and the effect of high dependency on the compressive domain in the DP model, we use a smaller angle of friction for the DP model in comparison with that of MDP. The yield stress and inelastic strain of DP and MDP models are given in tabulated manner in Table A2 in Appendix whereas the plasticity properties of CDP for differing tensile and compressive strengths are summarized in Table A3. These values have been obtained from the aforementioned literatures.

3.4 Projectile simulation

To simulate the drop of impact mass, elastic material properties of which are similar to those of steel reinforcement, from an elevated position, all nodes are given a common velocity (6.5 m/s) in a direction perpendicular to the slab surface. Therefore, the projectile strikes the slab at a constant velocity 6.5 m/s, the value of which is as given in Sangi and May (2009) and Chen and May (2009).

4. Result and discussion

In order for the finite element simulation to provide a sensibly accurate result, a sufficiently refined finite element mesh should be used. Therefore, the mesh density sensitivity is first carried out for the three considered material models for the determination of the optimal number of elements to be used for further investigation thereafter. The model specifications for aforementioned purpose are summarized in Table 3. Note that the numbers of elements and nodes for reinforcement bars and projectile remain constant since the intention here is to examine the mesh density effect of the plain slab only. For comparison, the measured and computed impact force-time relationships can be seen in Fig. 2. Since it is found in the current study that the MDP model follows very much the same response as that shown by the DP model, the result from only Mesh II of MDP (labeled as MDP) is shown in the figure. It is interesting to notice that Mesh II of both DP and MDP models, an intermediately dense amongst three meshes used, give somewhat the best replication of the impact-time response from measurement. Both computational models track reasonably well the measured impact force history in terms of the response outline, missing however the horizontal shift of that given by the latter. The experimental response, especially at the first two force history peaks, displays somewhat slower force dissipation, and therefore attributable to a wider spectrum of impact force transferring compared with that found in simulation. Nevertheless, the modeled impact force history plateau and response thereafter subsequent to these two peaks are by inspection in good agreement with the experimental result. On closer inspection, the behavior of dynamic loading in RC slab computed using the MDP is the best in comparison and closely reproduces that shown by the experiment. Therefore, we focus solely on the use of the MDP material model for further investigation in the remainder of the paper. It is worth mentioning that Mesh I and Mesh III of both DP and CDP models, though differ in magnitudes, are able to approximate a similar shape of impact force history produced by the experimental study. In general, their response magnitudes are respectively higher and lower than that of measured. As cultivating as this may seem, we would like to proceed, without pursuing the matter in concern, our investigation using the MDP model with Mesh II although it may be postulated at this point that a damping effect may contribute to such observations. Increases in the mesh density in all models bring the force-time responses to converge to magnitudes lower than that measured. A higher tendency to damp the impact force is observed as the element number increases, due to a high energy absorbing capability. Such observation can be linked to the nature of solid element used in the present models, which is of linear type, suggesting the use of higher order element that is more computationally expensive. The projectile velocity, which may not be constant in experiment, inaccurate capturing of exact load and boundary conditions as well as the variation in the material parameters can nevertheless play major role in this regard. Such consideration may be treated as the subject of future study.

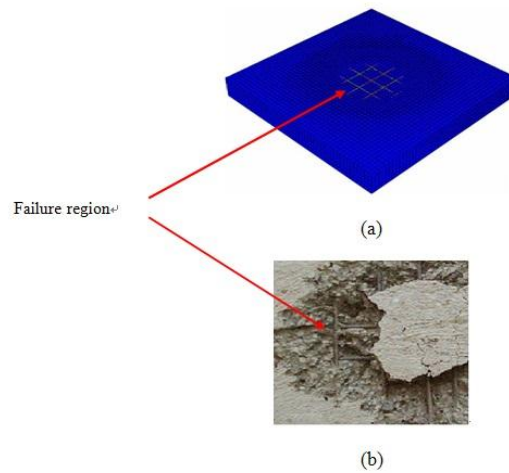


Fig. 3 Perforated and failure regions exposing the steel reinforcements: (a) model (b) experiment

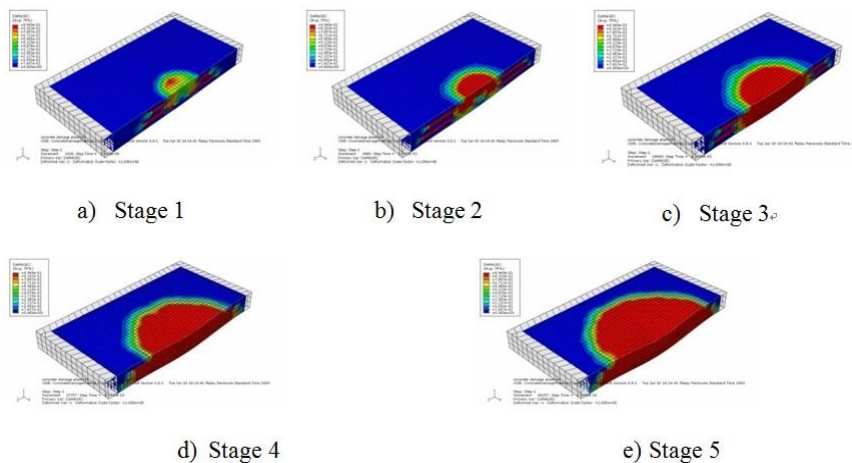


Fig. 4 Damage wave propagation between 0 s to 0.015 s

To facilitate the comparison between numerical model and experiment, Fig. 3 shows the failure profiles of slabs after impact. Focusing and examining the impacted regions, it is interesting to see that the numerical model exhibits reasonably close resemblance to that demonstrated by the experimental work. Particularly of interest is the high stress zones found in the reinforcement which agree with those of experiment where the concrete material is perforated exposing the steel bars as the highly stressed component in the impacted area.

Fig. 4 shows the sequential progress of the damage wave propagation from the initial potential damaged region under the zone of impact towards the supports. It is important to note that the simulation is able to demonstrate the deformation that occurs within a split of second, the motion

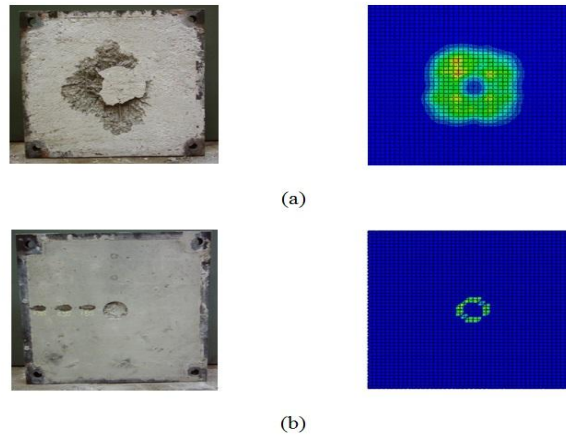


Fig. 5 A comparison of modeled final failure patterns of the impacted reinforced concrete slab with those measured by Chen and May (2009): (a) bottom face (b) top face

of which is otherwise costly to capture in an experiment using a high speed recording device. We can see clearly the accumulation of damage and perforation formed, initially from the impacted site, and then traversed in an outward spreading manner towards the supports. In Fig. 4 (d) and (e), a larger area of crack appears at the bottom of the slab and propagates, covering almost the whole slab including the area at the top centre, a direct indication of high tensile zone exceeding that of the cracking strain of concrete.

To investigate the detail of failure after impact, the final perforation patterns obtained from the experimental work and simulation are compared in Fig. 5. It can be seen in Fig. 5(a) that the shape of the perforated region at the bottom face of the slab resembles that of a ring: the outer diameter of the region is approximately 400 mm, and the inner diameter is approximately 180 mm. The simulated final failure pattern correlates well to the experiment with an exception that the latter has unperturbed portion on the right side of impacted area. It is essential to state here that although the inner diameter of the simulated failure zone is smaller than that of experiment, the outer diameter agrees very well. Observe in Fig. 5(b) that the general outlines of damage after impact from both surfaces are in close agreement. Although it is outside the scope of currently conducted study, it is worthy of emphasis that the disagreement displayed in the comparison may be contributed by an imperfect impact process generated from non-uniform surfaces contact in the experiment, which is likely coming from an unaligned loading environment and not entirely flat materials surfaces, and thus producing an asymmetrical damage pattern as shown in Fig. 5(a). This is in contrast with a highly symmetrical failure profile, as found in the simulation.

5. Conclusions

An impact of high mass and low velocity projectile on reinforced concrete slab is simulated in the ABAQUS/Explicit environment adopting three material descriptions: Drucker-Prager (DP), modified Drucker-Prager (MDP), and concrete damaged plasticity (CDP). In general, the ABAQUS model, with a reasonably dense mesh, is capable to model the impact response with a

satisfactory accuracy when compared to the results obtained from measurement. This is supported by good agreements achieved in the comparisons of impact force-time response and impact wave propagation behavior which includes also the general perforation formation and spreading. In addition, the failure profiles of the top and bottom faces of RC slab are quantitatively conformed to the observation found from experiment.

References

- ABAQUS/Explicit User's Manual, (2007), Version 6.7, Hibbitt, Karlsson & Sorensen, Inc.
- Abbas, H., Gupta, N.K. and Alam, M. (2004), "Nonlinear response of concrete beams and plates under impact loading", *Int. J. Impact Eng.*, **30**(8-9), 1039-1053.
- Agardh, L. and Laine, L. (1999), "3D FE-simulation of high-velocity fragment perforation of reinforced concrete slabs", *Int. J. Impact Eng.*, **22**(9-10), 911-922.
- Balakrishnan, S. and Murray, D.W. (1986), "Finite element prediction of reinforced concrete behavior", Struct. Engrg. Rep. No. 138, University of Alberta, Edmonton, Alberta, Canada.
- Chen, X.W., Li, X.L., Huang, F.L., Wu, H.J. and Chen, Y.Z. (2008), "Normal perforation of reinforced concrete target by rigid projectile", *Int. J. Impact Eng.*, **35**(10), 1119-1129.
- Chen, Y. and May, I.M. (2009), "Reinforced concrete members under drop-weight impacts", *Proceedings of the Institution of Civil Engineers: Structures and Buildings*, **162**(SB1), 45-56.
- Corbett, G.G., Reid, S.R. and Johnson, W. (1996), "Impact loading of plates and shells by free-flying projectiles: A review", *Int. J. Impact Eng.*, **18**(2), 141-230.
- DiMaggio, F.L. and Sandler, I.S. (1971), "Material model for granular soils", *J. Eng. Mech. Div.*, **97**, 935-950.
- Elwi, A. and Hruday, M. (1989), "Finite element model for curved embedded reinforcement", *J. Eng. Mech.*, **115**(4), 740-757.
- Gilbert, R.I. and Warner, R.F. (1978), "Tension stiffening in reinforced concrete slabs", *ASCE J. Struct. Div.*, **104**(12), 1885-1900.
- Gomes, H.M. and Awruch, A.M. (2001), "Some aspects on three-dimensional numerical modelling of reinforced concrete structures using the finite element method", *Adv. Eng. Software*, **32**(4), 257-277.
- Hand, F.R., Pecknold, D.A. and Schnobrich, W.C. (1973), "Nonlinear layered analysis of RC plates and shells", *ASCE J. Struct. Div.*, **99**(7), 1491-1505.
- Islam, M. J., Liu, Z. and Swaddiwudhipong, S. (2011), "Numerical study on concrete penetration/perforation under high velocity impact by ogive-nose steel projectile", *Comput. Concrete*, **8**(1), 111-123.
- Jofriet, J.C. and McNeice, G.M. (1971), "Finite element analysis of reinforced concrete slabs", *ASCE J. Struct. Div.*, **97**(3), 785-806.
- Lin, C.S. and Scordelis, A.C. (1975), "Nonlinear analysis of RC shells of general form", *ASCE J. Struct. Div.*, **101**(3), 523-538.
- Luccioni, B.M. and Luege, M. (2006), "Concrete pavement slab under blast loads", *Int. J. Impact Eng.*, **32**(8), 1248-1266.
- Naaman, A.E. and Gopalaratnam, V.S. (1983), "Impact properties of steel fibre reinforced concrete in bending", *Int. J. Cement Compos. Lightw. Concrete*, **5**(4), 225-233.
- Ong, K.C.G., Basheerkhan, M. and Paramasivam, P. (1999), "Resistance of fibre concrete slabs to low velocity projectile impact", *Cement Concrete Compos.*, **21**(5-6), 391-401.
- Phillips, D.V. and Zienkiewicz, O.C. (1976), "Finite element non-linear analysis of concrete structures", *Proc. Inst. Civ. Eng.*, **61**, 59-88.
- Rashid, Y.R. (1968), "Ultimate strength analysis of prestressed concrete pressure vessels", *Nucl. Eng. Des.*, **7**(4), 334-344.
- Rousseau, J., Frangin, E., Marin, P. and Daudeville, L. (2009), "Multidomain finite and discrete elements method for impact analysis of a concrete structure", *Eng. Struct.*, **31**(11), 2735-2743.

- Sangi, A.J. and May, I.M. (2009), "High-mass, low velocity impacts on reinforced concrete slabs", *7th European LS-DYNA Conference*, DYNAmore GmbH.
- Sawamoto, Y., Tsubota, H., Kasai, Y., Koshika, N. and Morikawa, H. (1998), "Analytical studies on local damage to reinforced concrete structures under impact loading by discrete element method", *Nucl. Eng. Des.*, **179**(2), 157-177.
- Scanlon, A. and Murray, D.W. (1974), "Time-dependent reinforced concrete slab deflections", *ASCE J. Struct. Div.*, **100**(9), 1911-1924.
- Shiu, W., Donze, F.V. and Daudeville, L. (2009), "Influence of the reinforcement on penetration and perforation of concrete targets: A discrete element analysis", *Int. J. Comput. Aid. Eng.*, **26**(1-2), 29-45.
- Tahmasebinia, F. (2008), "Finite element simulation of reinforced concrete structures under impact accident", *Struct. Survey*, **26**(5), 445 - 454.
- Tai, Y.S. and Tang, C.C. (2006), "Numerical simulation: the dynamic behavior of reinforced concrete plates under normal impact", *Theor. Appl. Fract. Mech.*, **45**(2), 117-127.
- Teng, T.L., Chu, Y.A., Chang, F.A. and Chin, H.S. (2004), "Simulation model of impact on reinforced concrete", *Cement Concrete Res.*, **34**(11), 2067-2077.
- Teng, T.L., Chu, Y.A., Chang, F.A. and Shen, B.C. (2005), "Penetration resistance of reinforced concrete containment structures", *Annal. Nucl. Energy*, **32**(3), 281-298.
- Zienkiewicz, O.C., Owen, D.R.J., Phillips, D.V. and Nayak, G.C. (1972), "Finite element methods in the analysis of reactor vessels", *Nucl. Eng. Des.*, **20**(2), 507-541.
- Zineddin, M. and Krauthammer, T. (2007), "Dynamic response and behavior of reinforced concrete slabs under impact loading", *Int. J. Impact Eng.*, **34**(9), 1517-1534.

Appendix

Table A1 Plastic hardening parameters for steel reinforcement

Yield stress [Pa]	Plastic strain
304600000	0
344190000	0.0244
385510000	0.0951
450390000	0.1384
470280000	0.191
500000000	0.2324
580000000	0.2728

Table A2 Drucker-Prager hardening parameters

Yield stress[Pa]	Inelastic strain
13000000	0
20000000	0.0007
24000000	0.001
37500000	0.002
22500000	0.0034
16000000	0.05

TableA 3 Additional concrete damaged plasticity (CDP) model parameters

Compressive behavior				
Yield stress [Pa]	Main-option		Sub-option	
	Inelastic strain	Rate	Damage parameter	Inelastic strain
			0	0
13000000	0	1.5	0	7.47307E-005
20000000	0.0007	1.5	0	9.88479E-005
24000000	0.001	1.5	0	0.000154123
37500000	0.002	1.5	0	0.000761538
22500000	0.0034	1.5	0.195402	0.002557559
16000000	0.05	1.5	0.596382	0.005675431
			0.894865	0.011733119
Tensile behavior				
Yield stress [Pa]	Main-option		Sub-option	
	Cracking strain	Rate	Damage parameter	Inelastic strain
3500000	0	1.5	0	0
1750000	0.00015	1.5	0	3.333E-005
800000	0.00035	1.5	0.406411	0.000160427
250000	0.0006	1.5	0.69638	0.000279763